J Stat Phys (2010) 141: 1039–1054
DOI 10.1007/s10955-010-0079-5

The Spectrum of the Billiard Laplacian of a Family of Random Billiards

Renato Feres · Hong-Kun Zhang

Received: 15 August 2010 / Accepted: 14 October 2010 / Published online: 9 November 2010
© Springer Science+Business Media, LLC 2010

Abstract *Random billiards* are billiard dynamical systems for which the reflection law giving the post-collision direction of a billiard particle as a function of the pre-collision direction is specified by a Markov (scattering) operator P. *Billiards with microstructure* are random billiards whose Markov operator is derived from a "microscopic surface structure" on the boundary of the billiard table. The microstructure in turn is defined in terms of what we call a *billiard cell* Q, the shape of which completely determines the operator P. This operator, defined on an appropriate Hilbert space, is bounded self-adjoint and, for the examples considered here, a Hilbert-Schmidt operator. A central problem in the statistical theory of such random billiards is to relate the geometric characteristics of Q and the spectrum of P. We show, for a particular family of billiard cell shapes parametrized by a scale invariant curvature K (Fig. 2), that the billiard Laplacian $P - I$ is closely related to the ordinary spherical Laplacian, and indicate, by partly analytical and partly numerical means, how this provides asymptotic information about the spectrum of P for small values of K. It is shown, in particular, that the second moment of scattering about the incidence angle closely approximates the spectral gap of P.

Keywords Billiards · Knudsen law · Spectral gap · Classical scattering

1 Introduction and main results

In the highly idealized classical scattering experiment shown in Fig. 1, a macroscopically flat surface in dimension 2 with a periodic, piecewise smooth, "molecular contour" is probed by a billiard particle and the angle of scattering is recorded as a function of the angle of incidence. The interaction between particle and surface consists of elastic collisions. The angle

R. Feres (✉)
Department of Mathematics, Washington University, Campus Box 1146, St. Louis, MO 63130, USA
e-mail: feres@math.wustl.edu

H.-K. Zhang
Department of Mathematics & Statistics, University of Massachusetts, Amherst, MA 01003, USA

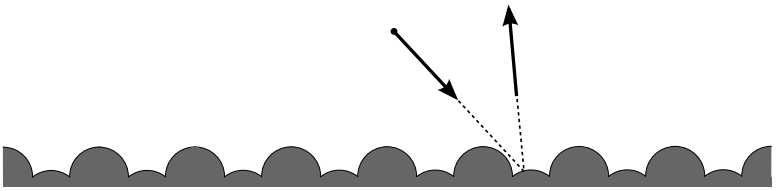

Fig. 1 An idealized scattering experiment

of incidence is under experimental control, but the precise position at which the particle hits the microscopic surface contour is random. The scattered angle is then a random function of the incidence angle, and the transition probabilities operator P describing the scattering process, to be defined shortly, depends canonically on the microscopic contour. The operator P gives rise to a class of Markov chains with continuous state space. Such a chain may be interpreted as a sequence of random directions of a billiard particle undergoing random flight inside a 2-dimensional channel whose boundary consists of two parallel lines with a given microstructure.

We henceforth refer to P as the *Markov operator* of the surface microstructure. One of the central questions in the theory of Markov chains with general state space is to describe, given such a P, its stationary distribution (or distributions, if it is not ergodic) and estimate the speed of convergence to stationarity. It can be shown under very general assumptions on the microstructure [4] that the stationary probability of scattered angles is unique and is given by the well-known *Knudsen cosine law*, $d\nu(\varphi) = \frac{1}{2}\cos\varphi\, d\varphi$ (the normalization constant $1/2$ is for dimension 2), where φ measures angles relative to the normal to the (macroscopically flat) surface. This is the case regardless of the shape of the microstructure. (For an experimental view of the cosine law, it is interesting to go back to Knudsen's now classical work. See, for example, [6].) The stationary distribution is a universal feature of these kinds of systems at equilibrium, independent of the details of the interaction related to the geometric features of the given billiard microstructure.

On the other hand, it can be expected that such properties of the Markov process as mixing times and decay of correlations depend on those detailed features. Properties of the Markov chain pertaining to relaxation to equilibrium are related to spectral properties of P. The main concern of this paper is to investigate the spectrum of P for the specific family of microstructures shown in Fig. 2. (We like to think of this family, for varying K, as representing the "molecular structure" of a surface made of closely packed discs of a fixed radius, which is then probed by different species of billiard gas molecules of different radii. By varying the radius of the gas molecules, the effective curvature of the surface contour is changed accordingly. In this sense, the spectral properties of P are characteristics of the interaction rather than intrinsic properties of the surface itself.)

The Markov operator can be defined on the Hilbert space $L^2((-\pi/2, \pi/2), \nu)$ of square-integrable functions on the set of scattered angles with the stationary probability measure ν, and it turns out to be a bounded self-adjoint operator with nice spectral properties. For example, it is shown in [4], under fairly general conditions, that Sinai-type [7] billiard cells (see Fig. 3 for the definition of a billiard cell) correspond to compact (Hilbert-Schmidt) operators. Throughout the rest of the paper, we find it convenient to use angle conventions as described in Fig. 3. The Hilbert space is now $L^2([0, \pi], \nu)$ and the "cosine law" becomes

Fig. 2 A simple billiard microstructure consisting of arcs of circle. We refer to it as the *bumps family*. The (scale-invariant) curvature of the bumps is defined by $K = L/R$, where L is the distance between two consecutive corner points and R is the radius of the circular arcs. We assume throughout, without loss of generality, that $L = 1$. This paper is concerned with properties of this particular family, as a function of K, for small values of K. A billiard cell is indicated by the *dashed lines*

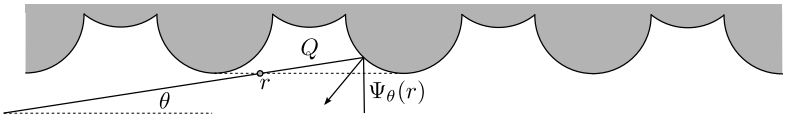

Fig. 3 The microstructure around a collision point on the boundary of a billiard table. The billiard cell is denoted Q. It is the unit of pattern of the periodic structure. A billiard particle enters a cell with angle $\theta \in (0, \pi)$ at a position $r \in [0, 1]$ and leaves it at an angle $\Psi_\theta(r)$. The random reflection law is defined by the condition that r is a uniform random variable over $[0, 1]$. The specific shape that is the focus of our work is shown in Fig. 2

$d\nu(\theta) = \frac{1}{2} \sin\theta \, d\theta$. Then P takes the form

$$(Pf)(\theta) = \int_0^1 f(\Psi_\theta(r)) \, dr. \tag{1.1}$$

Information about the rate of convergence to stationarity can be read from the spectrum of P. Of special interest in this regard is the so-called *spectral gap* which, for the purposes of this paper, can be defined as the distance between the top eigenvalue of P, namely 1, and the second largest eigenvalue. For our systems, 1 is a simple eigenvalue and the spectral gap is positive [4]. In this case, the gap provides an estimate of the exponential rate of convergence of some initial distribution of angles to the invariant distribution ν under iterates of P. As will be described in another paper, the spectrum of P is also needed for a precise determination of the diffusion constant of a (Knudsen) gas of billiard particles inside channels. (In a Knudsen gas, molecules only collide with the wall of the container, or channel, and not among themselves.)

Estimates of the spectral gap for Markov operators are often done by the coupling method of probability theory and one typically obtains information about the second eigenvalue only. We show, for the bumps family of Fig. 2, that the spectral theory of P can be described very explicitly when the curvature parameter K is small.

Figure 4 shows the graph of the spectral gap as a function of the scale-invariant curvature parameter K for the family of Fig. 2, obtained by numerical simulation of the billiard dynamics. The salient feature of the graph that one would like to explain in analytic terms and understand in terms of particle scattering properties is that, for relatively small values of K, the function is very well approximated by

$$\gamma(K) = \frac{K^2}{3} + \mathcal{O}(K^3).$$

We return to this point in Sect. 2.

The main observation of the paper, Theorem 1, is that the self-adjoint operator P is very directly related to the spherical Laplacian, which will allow us to obtain asymptotic information about the full spectrum of P, not only the spectral gap γ. Before stating the

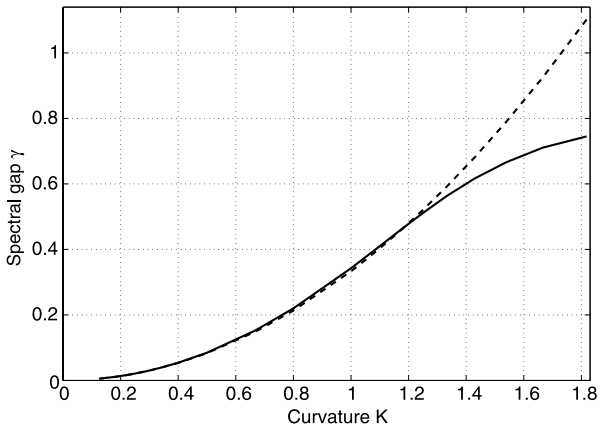

Fig. 4 The spectral gap of the Markov operator for the family of microstructures of Fig. 2 is given, as a function of the curvature parameter K, for small values of K, by $\gamma(K) = K^2/3 + \mathcal{O}(K^3)$. The *dashed line* above is the graph of $K^2/3$, and the *solid line* is the graph of $\gamma(K)$ obtained by numerical simulation of the billiard map and by numerical evaluation of the top eigenvalues

theorem, it is helpful to make the following simple observation concerning the billiard map associated to the microstructure.

The function $\Psi_\theta(r)$ is the angular component of the return billiard map to the entrance segment of Q (represented by one of the dashed lines in Fig. 3). This segment will be identified with the interval $[0, 1]$. Let $M = [0, 1] \times [0, \pi]$ be the phase space of the billiard system on Q, restricted to this special segment. The return billiard map to M is well-defined and smooth on an open set of full measure of M, due to Poincaré recurrence and general properties of billiard systems. We denote this map by $T : M \to M$. The T-invariant (Liouville) probability measure on M is the measure η such that

$$d\eta(r, \theta) = \frac{1}{2} \sin\theta \, dr \, d\theta.$$

The images of the points $(r, 0)$ and (r, π) under T are not well-defined, although we can write $\Psi_0(r) = 0$ and $\Psi_\pi(r) = \pi$ for all r. This ambiguity is eliminated by regarding T as a map on the sphere S^2, as follows. First, we consider r as a coordinate function of the circle S^1, so that $[0, 1] \times [0, \pi]$ can be viewed as parametrizing the cylinder $S^1 \times [0, \pi]$. By collapsing each boundary circle of the cylinder to a point we obtain a topological sphere, and T becomes a well-defined invertible map of the sphere S^2 to itself. The correspondence $(s, \theta) \mapsto (\theta, \phi)$, where $\phi = 2\pi r$, translates the billiard coordinates into the standard spherical coordinates. (See Fig. 5.)

This is more than a topological remark, however, since the invariant measure η corresponds to the normalized area measure on S^2. Therefore, the billiard map T is naturally regarded as an area-preserving map of the 2-sphere with its standard metric. We interpret $2\pi r$ and θ as the longitude and latitude coordinates on S^2, respectively, and the collapsed boundary circles of the cylinder as the north and south poles, both fixed points under T. Therefore, T induces in a natural way a unitary operator on $L^2(S^2, A)$, where A is the normalized area measure on the unit sphere, given by $f \mapsto f \circ T$.

Similarly, the Markov operator P corresponds to a self-adjoint (if Q is symmetric) operator on $L^2(S^2, A)$, obtained by post-composing T with the averaging operator over the group of rotations about the north-south axis. Thus it is reasonable to expect that spherical harmonics should play a role in the study of the spectrum of P. The main result of this paper makes the connection explicit by relating P and the spherical Laplacian.

The following theorems refer to the family of billiard cells shown in Fig. 2. Let $\mathcal{F}(S^2)$ represent the space of smooth real valued functions on S^2 that are invariant under the group

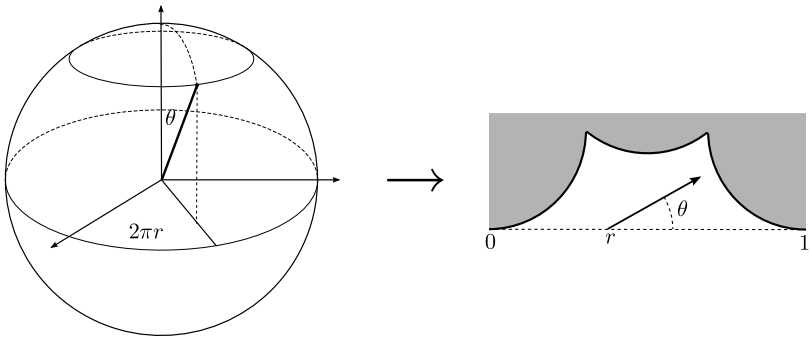

Fig. 5 The initial state of a billiard trajectory in the cell Q is parametrized by a point on the unit sphere S^2. Under this correspondence, the return billiard map to the entrance segment of ∂Q (the *dashed line* on the right) becomes an area preserving invertible map of S^2

G of rotations about the North-South axis. This is a dense subspace of the closed subspace of G-invariant square-integrable functions on S^2. The *discrete Laplacian* associated to the operator P is simply $L := P - I$, where I is the identity map, and the spherical Laplacian restricted to $\mathcal{F}(S^2)$ is the differential operator

$$\Delta\Phi = \frac{1}{\sin\theta}\frac{d}{d\theta}\left(\sin\theta\frac{d\Phi}{d\theta}\right).$$

Theorem 1 refers to the angle θ_0, defined as $\theta_0 = 3\beta/2$, where β is shown in Fig. 9. This angle satisfies

$$\theta_0 = 3K/2 + \mathcal{O}(K^3).$$

Let $S^2_{\theta_0}$ represent a spherical band in S^2 spanning the latitudes $(\pi/2-\theta_0)$ South to $(\pi/2-\theta_0)$ North, that is, the set given by $\sin\theta \geq \sin\theta_0$.

Theorem 1 *Let Q be a billiard cell in the family of circular bumps microstructures shown in Fig. 2, having curvature parameter K, and let $\Phi \in \mathcal{F}(S^2)$. Then*

$$P\Phi - \Phi = \frac{K^2}{6}\Delta\Phi + \mathcal{O}(K^3)$$

over the set $S^2_{\theta_0}$.

The proof of Theorem 1 is based on an analysis of the *moments of scattering*, defined as follows. Recall that the angle $\Theta = \Psi_\theta(r)$ is viewed as a random variable by assuming that r is a uniform random variable over $[0, 1]$. Since we are assuming that K is small, the distribution of Θ should be concentrated near θ. To measure this concentration we define the jth *moment of scattering*, $j = 0, 1, \ldots$, by

$$\mathcal{E}_j(\theta) := E[(\Theta - \theta)^j] = \int_0^1 (\Psi_\theta(r) - \theta)^j \, dr,$$

where E denotes expectation. We also define $\overline{\mathcal{E}}_j(\theta) := E[|\Theta - \theta|^j]$. The next theorem contains the main technical fact of the paper, which is based on an elementary geometric analysis of the billiard trajectories going in and out of Q.

Theorem 2 *The following properties hold for the moments of scattering, $\mathcal{E}_j(\theta)$, and the mean deviations from the incidence angle, $\overline{\mathcal{E}}_j(\theta)$, $j = 0, 1, \ldots$, for the circular bumps family of Fig. 2 with scale-free curvature parameter K. Let $\theta_1 = \beta/2$ and $\theta_0 = 3\beta/2$, where β is the corner angle of the bumps geometry* (*see Fig. 9*).

1. *For $\theta \in [0, \pi]$, $\mathcal{E}_j(\pi - \theta) = (-1)^j \mathcal{E}_j(\theta)$. Thus it is sufficient to consider angles in $[0, \pi/2]$.*
2. *If $\theta \in [\theta_0, \pi/2]$, then*

$$\mathcal{E}_j(\theta) = \begin{cases} K^j/(j+1) + \mathcal{O}(K^{j+2}) & \text{if } j \text{ is even,} \\ K^{j+1} \cot\theta/2(j+2) + \mathcal{O}(K^{j+3}) & \text{if } j \text{ is odd.} \end{cases}$$

   (*Exact formulas for the $\mathcal{E}_j(\theta)$ over this range of angles are shown in the proof in Sect. 5.*)
3. *If $\theta \in [0, \pi/2]$, then*

$$\overline{\mathcal{E}}_j(\theta) \leq \begin{cases} (2K)^j + \mathcal{O}(K^{j+2}) & \text{if } \theta_1 \leq \theta \leq \pi/2, \\ (9K \sin\theta)^{j/2} & \text{if } \theta < \theta_1. \end{cases}$$

   Roughly, $\overline{\mathcal{E}}_j(\theta) = \mathcal{O}(K^j)$, and as θ goes to 0 for a fixed K, $\overline{\mathcal{E}}_j(\theta) = \mathcal{O}(\theta^{j/2})$.

Theorem 1 is a straightforward application of the above theorem about the moments. In fact, let Φ be smooth real valued function on $(0, \pi)$. The supremum of the kth derivative of Φ will be written $\|\Phi^{(k)}\|$. Then by Taylor's theorem

$$(P\Phi - \Phi)(\theta) = \sum_{k=1}^{n} \mathcal{E}_k(\theta) \frac{\Phi^{(k)}(\theta)}{k!} + R_n(\theta), \tag{1.2}$$

where the error term satisfies $|R_n(\theta)| \leq \overline{\mathcal{E}}_{n+1}(\theta) \|\Phi^{(n+1)}\|/(n+1)!$. Retaining terms of degree two or less and applying Theorem 2 we find

$$(P\Phi - \Phi)(\theta) = \frac{K^2}{6} \left(\cot\theta \Phi'(\theta) + \Phi''(\theta)\right) + \mathcal{O}(K^3) = \frac{K^2}{6} \Delta\Phi(\theta) + \mathcal{O}(K^3). \tag{1.3}$$

The proof of Theorem 2 will be given in Sect. 5.

2 The Spectrum of P

We now turn to the spectrum of P. The following observations are supported by numerical calculations as shown below. We do not give precise mathematical justifications for them at this point. The details of a spectral perturbation argument starting from Theorem 1, which we need to more precisely state and prove the following claims, will be given in another paper.

Recall that

$$\frac{1}{\sin\theta} \frac{d}{d\theta} \left(\sin\theta \frac{d\Phi}{d\theta}\right) + l(l+1)\Phi = 0$$

is the *Legendre equation* and its canonical solutions for integers $l \geq 0$ are the *Legendre functions* Φ_l, of which the first few are: $\Phi_0(\theta) = 1$, $\Phi_1(\theta) = \cos\theta$, $\Phi_2(\theta) = (3\cos^2\theta - 1)/2$.

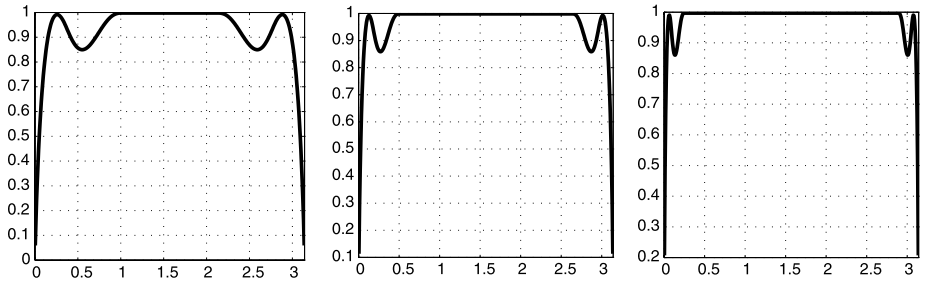

Fig. 6 Ratio $\mathcal{E}_2(\theta)/\gamma(K)$ as function of θ. From left to right: $K = 2/3, 1/3, 1/6$. The constant value in the middle region is very close to 1. This gives an asymptotic interpretation of the spectral gap $\gamma(K)$ of P as the mean-square dispersion of the post-collision angle around the pre-collision angle

For small values of K, Theorem 1 suggests that the Φ_l are approximate eigenfunctions of P with the following eigenvalues:

$$P\Phi_l \approx \left(1 - \frac{K^2}{6} l(l+1)\right) \Phi_l.$$

In particular, the numerical result described in Fig. 4 supports this remark, since the second eigenvalue of P (for $l = 1$) is

$$\lambda_2 = 1 - \gamma(K) \approx 1 - \frac{K^2}{3}$$

with associated eigenfunction being approximately $\Phi_1(\theta)$.

Especially noteworthy is the relationship between the second moment of scattering and the spectral gap for $\sin\theta > \sin\theta_0$:

$$\mathcal{E}_2(\theta)/\gamma(K) \approx 1.$$

The approximation is very good, as can be observed in Fig. 6. In fact, in the middle range of angle values in Fig. 6, $\mathcal{E}_2(\theta)$ and $\gamma(K)$ look nearly identical, even for K not much smaller than 1.

Because of this close connection between the second moment and the spectral gap, it is worth highlighting an exact expression for $\mathcal{E}_2(\theta)$ for $\sin\theta \geq \sin\theta_0$:

$$\begin{aligned}\mathcal{E}_2(\theta) &= 8K^2 \int_0^{\arcsin(K/2)/K} \cos(Ks) s^2 \, ds \\ &= 4 \arcsin(K/2) \left(\arcsin(K/2) + 4 \frac{\sqrt{1 - (K/2)^2}}{K} \right) - 8.\end{aligned}$$

This expression can be derived from the proof of Theorem 2. Notice how the second moment is constant over this entire middle range of angles, corresponding to the flat plateau in the graphs of Fig. 6. (This is a common feature of the even moments. The odd moments have the form $A_j \cot\theta$ for some constant A_j. See (5.3).) As an illustration, for $K = 2/3$ we find $\mathcal{E}_2(\theta) = 0.1516$, whereas $\gamma(2/3) = 0.1519$, obtained from a finite rank approximation of P via numerical simulation of the billiard map.

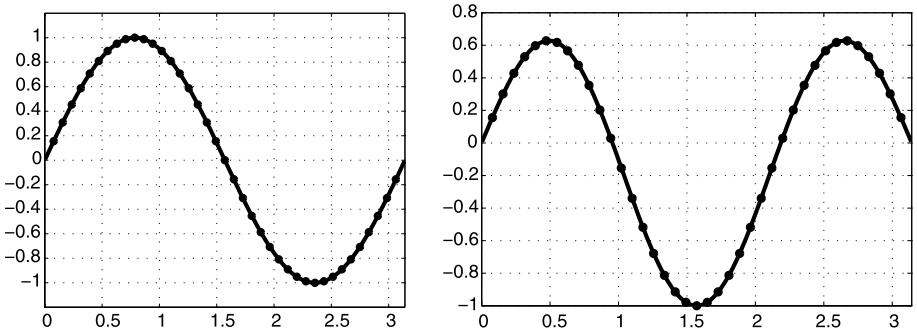

Fig. 7 Comparison of the second and third left-eigenfunctions of P (*solid line*) and $\Phi_j(\theta)\sin\theta$ (*dots*), for $j = 1, 2$ and $K = 1/6$. A finite rank approximation of the (compact) operator P was obtained by numerical simulation of the billiard map, and the eigenfunctions were found numerically

As further evidence for the approximation of the eigenfunctions consider Fig. 7. In it we compare the second and third (left)-eigenfunctions of P (which may be called *eigendensities* of P. The first eigendensity is $\sin\theta$, so the exact and approximate functions coincide).

There are many questions raised by the above observations. One is the extent to which what is being described here is particular to the bumps family, or whether we are noting something more general. Clearly, the function $K^2/6$ that appears in front of the spherical Laplacian Δ in the approximation of $P - I$ of Theorem 1 is specific to the example at hand, but there is numerical evidence, based on other microstructure shapes with small moments of scattering, that Δ should play a central role in more general situations. We note that the case of large K is being studied by very different methods by the authors, and an estimate of the spectral gap is obtained; and an application of the present results to the estimation of the diffusion constant of a Knudsen gas in channels (essentially proving a central limit theorem for the Markov operator P) is also work in progress by the authors.

Another basic problem is to understand how the above ideas can be carried out for microstructures in dimension 3. One reason that spherical harmonics play a role in the two-dimensional scattering problem is hinted at by the fact noted above that the deterministic billiard map T is an area preserving map of the two-sphere. It is less clear what similar space would be involved in the 3-dimensional version of the problem.

The question of speed of convergence to invariant measures under the iteration of certain operators associated to deterministic billiard systems, such as transfer operators, has been widely studied by many authors from a very different perspective. We mention [2, 8] for example. Since our Markov chains are canonically associated to a deterministic billiard, it may be hoped that some of the observations made here have relevance in the deterministic context.

3 Background on Random Billiards and Microstructures

For the general definitions and properties concerning deterministic billiard dynamical systems we refer to [1]. More information about properties of random billiards and the operator P that are mentioned in this paper without proof can be found in [4]. There is a fair amount of work concerning random billiards in the literature. We mention only [3] and references cited there as an example that is closely related to our viewpoint. The model we use here was first discussed in [5].

In the standard set up, a billiard (point) particle of a 2-dimensional billiard system moves with constant velocity in the interior of an open subset of the Euclidean plane having piecewise smooth boundary—the billiard table—and reflects off the boundary of the table according to the usual mirror reflection rule.

A *random billiard* is a probabilistic version of this general set up in which the mirror reflection law is replaced with some probabilistic reflection rule. Dropping for the moment the assumption that the system is 2-dimensional, let B denote the billiard table in $\mathbb{R}^n$, and suppose that x is a regular boundary point so that the tangent space to ∂B at x is defined, and $n(x)$ is the unit normal vector to the boundary at x pointing into B. Define H_x^+ (respectively, H_x^-) to be the set of non-zero vectors at x whose inner product with $n(x)$ is non-negative (respectively, non-positive). Then a general reflection law can be defined by the (measurable) assignment, for each regular point x in ∂B and each $v \in H_x^-$, of a probability measure μ_v on H_x^+.

One example of special interest in kinetic theory of gases is the already mentioned Knudsen cosine law. For this and the other examples in the paper, collisions do not change the speed of the billiard particle, so let $S^{\pm}$ denote the set of unit vectors in $H_x^{\pm}$ and define for each $v \in S^-$ a probability measure μ_v on H_x^+ that is independent of v and has density, relative to the area measure on S^+, proportional to the cosine of the angle between the direction of reflection and $n(x)$. We denote this reflection probability by ν, so that

$$d\nu(u) = C\langle u, n(x)\rangle dA(x),$$

where u is a unit vector in H^+, A is the ($(n-1)$-dimensional) area measure on S^+, and C is a normalization constant.

The following definition extends this example to a much more general, but very natural class of random billiard reflection laws. For simplicity, we denote by S either S_x^+ or S_x^- and also do not write the subscript if there is no possibility of confusion. Let $\mathcal{P}(S)$ be the space of probability measures on S. The reflection law is then a correspondence $v \in S \mapsto \mu_v \in \mathcal{P}(S)$. We still denote by ν the Knudsen law just defined.

Definition 3 (Elastic random reflection) We say that a random reflection rule is *elastic* if it is a correspondence $v \in S \mapsto \mu_v \in \mathcal{P}(S)$ with respect to which the Knudsen reflection law is stationary, that is,

$$\nu = \int_S \mu_u \, d\nu(u),$$

and reflection is *time-reversible* with respect to ν, that is,

$$d\mu_v(u)d\nu(v) = d\mu_{-u}(-v)d\nu(-u).$$

(This second condition implies the first.)

The motivation for this definition is that it identifies certain desirable properties that lend some physical plausibility, from the point of view of classical kinetic theory (in the absence of thermal effects), to any particular model of random billiard system we may like to consider for which the requirements of the definition can be ascertained. Also notice that ν is the angular part of the Liouville measure of a deterministic billiard system, so one may expect a system satisfying the definition to be in some way related to deterministic billiards.

Billiards with microstructure having bilaterally symmetric cells (that is, invariant under reflection on a line through the middle point of the entrance boundary segment of Q and

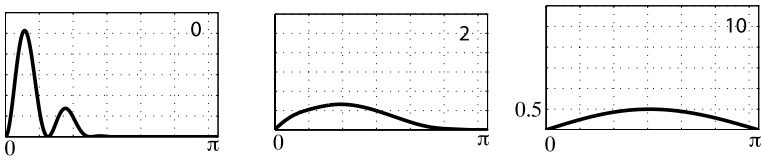

Fig. 8 The leftmost graph gives the density relative to the uniform distribution on $[0, \pi]$ of an arbitrary initial probability distribution μ. The *middle graph* gives μP^2, the distribution after two collisions, where P is the Markov operator associated to the microgeometry shown on Fig. 2. The *third graph* shows the density after 10 collisions. Notice that it approximates well the density of the stationary distribution, $d\nu(\theta) = \frac{1}{2}\sin\theta\, d\theta$. The spectrum of P as a function of the geometric parameter K provides information, for example, about the rate of convergence $\mu P^n \to \nu$. (The above curves were obtained by approximating P via numerical simulation of the billiard transformation)

perpendicular to it) are examples of systems with random elastic collisions (see [4]). They can be defined in much greater generality than we do here (or in [4], where one definition is stated more formally), so as to model non-periodic random scattering media in dimensions 2 or higher, but in the simplest form it consists of an ordinary billiard table B in dimension 2 together with a billiard cell Q, and the interaction is as described in Fig. 3. (The figure shows the microscopic view of the interaction between the billiard particle and the boundary of B, so the shape of B is not visible at this scale.) The scale of interaction is set by Q. Since the length scales of B and Q are not comparable, Q, and any geometric parameter associated to it that can affect the spectrum of P, such as curvatures, are only defined up to homothety. This incommensurability of B and Q motivates the definition of random reflection described in Fig. 3. For a given pre-collision velocity vector represented by the angle θ, the distribution of post-collision scattered angles is given by a measure μ_θ such that

$$\mu_\theta(A) = (\delta_\theta P)(A) = \int_0^1 \chi_A(\Psi_\theta(r))\, dr,$$

where A is any Borel subset of $[0, \pi]$ and δ_θ is the Delta measure supported at θ.

The fact that random reflection for a symmetric Q is elastic (according to Definition 3) implies that the associated Markov operator P is self-adjoint on $L^2([0, \pi], \nu)$. (See [4].) Recall that the operator acts on functions according to 1.1 and on signed measures by $(\mu P)(f) = \mu(Pf)$, where $\mu(g) := \int g\, d\mu$. In particular, invariance of ν is expressed by $\nu P = \nu$. If the microstructure is not symmetric, the adjoint of P is $P^* = JPJ$, where J is the unitary involution given by $Jf(\theta) = f(\pi - \theta)$. The L^2-norm of P is 1, so its spectrum is contained in $[-1, 1]$. It was shown in [4], and will be greatly elaborated in future paper, that P is compact for a wide range of shapes of Q.

It is easily seen numerically that the speed of convergence of μP^n to the stationary distribution ν varies greatly with the shape of Q. Figure 8 illustrates this convergence for the precise billiard contour shown in Fig. 2.

4 The Scattering Function Ψ_θ

For any bilaterally symmetric billiard cell shape, such as the one shown in Fig. 9, the identity

$$\pi - \Psi_\theta(r) = \Psi_{\pi-\theta}(1 - r) \tag{4.1}$$

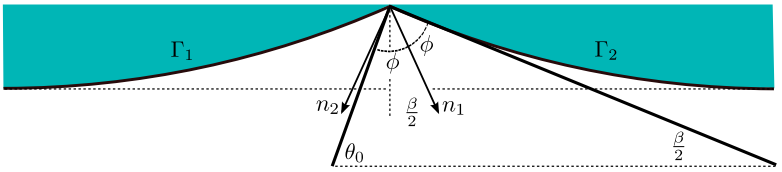

Fig. 9 The angle θ_0 represents the initial direction of a billiard trajectory that hits the corner point and reflects off Γ_1 at a grazing angle to Γ_2. This figure also shows the definition of β

holds. Thus one can generally assume that $\theta \leq \pi/2$. Results obtained over this range of angles can then be restated for $\theta > \pi/2$ by symmetry, using (4.1).

From this point on we deal specifically with the one-parameter family of billiard cells shown in Fig. 2. Let β denote the corner angle, i.e., the angle between the normal vectors, n_1 and n_2, to Γ_1 and Γ_2 at their intersection point. (See Fig. 9.) An elementary geometric arguments gives the relation

$$\frac{K}{2} = \sin\frac{\beta}{2}. \tag{4.2}$$

Also define θ_0 as the angle representing the initial direction of a billiard trajectory that reflects off Γ_1 at the corner point and leaves the billiard cell along the tangent direction to Γ_2 at the corner point. (See Fig. 9.) An examination of the angles shown in Fig. 9 gives

$$\theta_0 = \frac{3\beta}{2}. \tag{4.3}$$

Equation (4.3) and elementary trigonometry imply

$$\sin\theta_0 = \frac{3K}{2} - \frac{K^3}{2}. \tag{4.4}$$

The significance of θ_0 is that Ψ_θ is particularly simple when $\sin\theta \geq \sin\theta_0$ since, in this case, each billiard trajectory only collides once with the boundary of the billiard cell. Smaller values of θ will be considered below.

We sketch now some of the general properties of the graph of Ψ_θ for θ in this range of values. This is shown on Fig. 10. As already noted, there is no loss of generality in assuming that $0 < \theta \leq \pi/2$. When $\sin\theta \geq \sin\theta_0$ the function Ψ_θ has a jump discontinuity at

$$r_0 = \frac{1}{2} - \frac{1 - \sqrt{1 - \frac{K^2}{4}}}{K}\cot\theta = \frac{1}{2} - \frac{K}{8}\cot\theta + \mathcal{O}(K^3) \tag{4.5}$$

and over $(0, r_0)$ and $(r_0, 1)$ it is differentiable. The limit of $\Psi_\theta(r)$ as r approaches r_0 from the left is $\theta - \beta$, and the limit as r approaches r_0 from the right is $\theta + \beta$, as is easily verified. This is shown in Fig. 10. The incoming angle, θ, and the outgoing angle, $\Theta = \Psi_\theta(r)$, are seen to be related by

$$\cos\left(\frac{\theta + \Theta}{2}\right) - \cos\theta = \begin{cases} Kr\sin\theta & \text{if } r < r_0, \\ K(r-1)\sin\theta & \text{if } r > r_0. \end{cases} \tag{4.6}$$

It is convenient to express this equation in terms of the arc-length variable, s, on Γ_1 and Γ_2 instead of Θ. On both segments of circular arc, $s = \alpha/K$, where α ranges from 0 to $\beta/2$

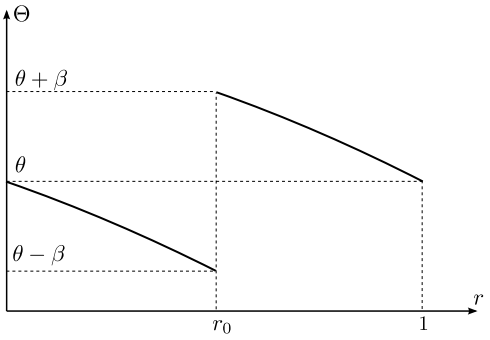

Fig. 10 A sketch of the graph of the function $\Theta = \Psi_\theta(r)$ for $\sin\theta \geq \sin\theta_0$. The parameters β and r_0 are described in the text

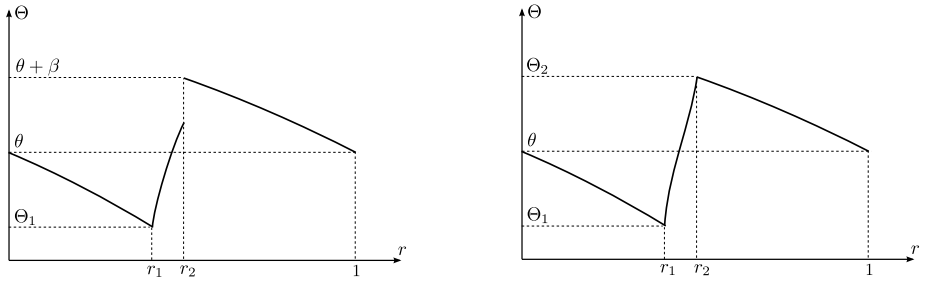

Fig. 11 For θ relatively shallow (close to 0 or π), Ψ_θ has an additional smooth piece. The sketch on the left corresponds to $\theta_1 := \beta/2 < \theta < \theta_0 = 3\beta/2$, and the one on the right corresponds to $\theta < \theta_1$. Similar graphs for θ in $(\pi - \theta_0, \pi - \theta_1)$ and $[\pi - \theta_1, \pi)$ are obtained by symmetry. An estimate for Θ_2 is given in the text

on both arcs. We are parametrizing the two arcs in such a way that $\alpha = \beta/2$ corresponds to the corner point, both over Γ_1 and over Γ_2. Notice that

$$\Theta = \begin{cases} \theta - 2Ks & \text{if } r < r_0, \\ \theta + 2Ks & \text{if } r > r_0. \end{cases} \tag{4.7}$$

It follows from this and (4.6) that

$$\cos\theta = \begin{cases} \cos(\theta - Ks) - Kr\sin\theta & \text{if } r < r_0, \\ \cos(\theta + Ks) + K(1-r)\sin\theta & \text{if } r > r_0. \end{cases} \tag{4.8}$$

In particular,

$$\Lambda(\theta, s)^{-1} := \frac{\partial s}{\partial r} = \begin{cases} \sin\theta/\sin(\theta - Ks) & \text{if } r < r_0, \\ -\sin\theta/\sin(\theta + Ks) & \text{if } r > r_0. \end{cases} \tag{4.9}$$

Notice that Λ is bounded away from 0 and ∞ since $\theta > \theta_0 = 3\beta/2$, if $\theta \leq \pi/2$, with a similar inequality if $\theta > \pi/2$.

It will be useful to consider some general features of Ψ_θ for *shallow* θ. By a shallow angle we mean θ such that $\sin\theta < \sin\theta_0$. Since it is sufficient to consider $\theta \leq \pi/2$, this means simply that $\theta < \theta_0$. If K is small enough, a billiard trajectory with initial angle θ may reflect off the boundary of the billiard cell more than once, but no more than twice. The graph of Ψ_θ is seen by inspection to have the qualitative features shown in Fig. 11. For a rough estimate of the range of scattered angles for a given shallow θ it will be sufficient to

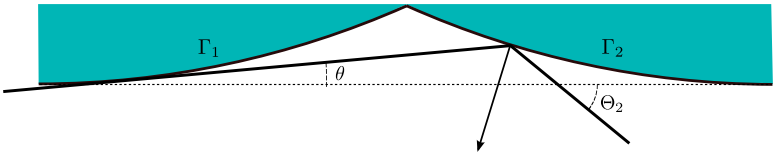

Fig. 12 Definition of the angle Θ_2. Compare with Fig. 11

estimate the angle Θ_2 shown on the graph on the right in Fig. 11. This is the exit angle of a billiard trajectory that enters the billiard cell at an angle θ, has a grazing collision with Γ_1 and reflects off Γ_2 before leaving the cell. (See Fig. 12.)

By elementary geometry (based on Fig. 12) it can be shown that θ and Θ_2 satisfy

$$\cos\left(\frac{\theta+\Theta_2}{2}\right) = 1 - K\sin\theta. \tag{4.10}$$

From this relation one derives the following estimate for Θ_2, where it is assumed that $K \le 1$:

$$\sqrt{8K\sin\theta} - \theta \le \Theta_2 \le a(K)\sqrt{8K\sin\theta} - \theta. \tag{4.11}$$

Here $a(K)$ satisfies $1 \le a(K) \le 1 + 0.05K^2$.

5 Moments of Scattering

The goal of this section is to prove Theorem 2, concerning the moments of scattering in terms of θ and K, for small K. We assume that $\sin\theta \ge \sin\theta_0$. As always, we do the calculations for $\theta \le \pi/2$. Notice that formula (4.1) implies that

$$\mathcal{E}_j(\pi - \theta) = (-1)^j \mathcal{E}_j(\theta) \tag{5.1}$$

which is the first claim of Theorem 2.

The contribution to the moments due to each differentiable branch of the function Ψ_θ can be written, by a change of variables, as $\pm\int_0^{\beta/2K} (\Theta(\theta,s)-\theta)^j \Lambda(\theta,s)\,ds$. From this and (4.7) and (4.9) one has

$$\mathcal{E}_j(\theta) = \int_0^{\beta/2K} \frac{\sin(\theta+Ks) + (-1)^j \sin(\theta - Ks)}{\sin\theta} (2Ks)^j\,ds. \tag{5.2}$$

After elementary algebraic manipulation this yields, for $j = 0, 1, \ldots,$

$$\mathcal{E}_j(\theta) = \begin{cases} 2^{j+1}K^j a_j & \text{if } j \text{ is even,} \\ 2^{j+1}K^j b_j \cot\theta & \text{if } j \text{ is odd,} \end{cases} \tag{5.3}$$

where $a_j = \int_0^{\beta/2K} \cos(Ks)s^j ds$ and $b_j = \int_0^{\beta/2K} \sin(Ks)s^j ds$. Recall that

$$\beta/2K = \arcsin(K/2)/K = \frac{1}{2} + \mathcal{O}(K^2). \tag{5.4}$$

Approximating the integrals results in

$$\mathcal{E}_j(\theta) = \begin{cases} K^j/(j+1) + \mathcal{O}(K^{j+2}) & \text{if } j \text{ is even,} \\ K^{j+1}\cot\theta/2(j+2) + \mathcal{O}(K^{j+3}) & \text{if } j \text{ is odd.} \end{cases} \tag{5.5}$$

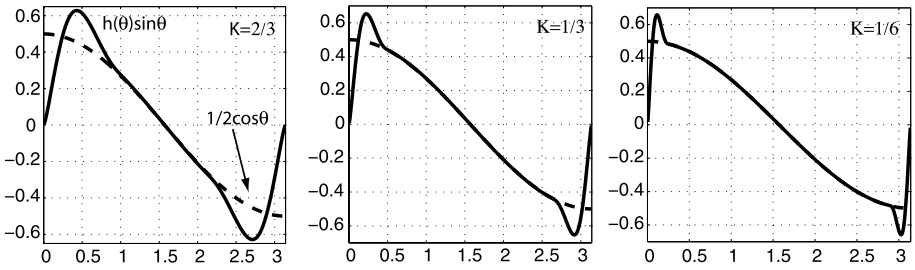

Fig. 13 Comparison of $\mathcal{E}_1(\theta)\sin\theta/\gamma(K)$ and $\frac{1}{2}\cos\theta$ for 3 values of K. The *horizontal axis* ranges from 0 to π and the *vertical axis* is dimension-free

We now give an upper bound for $\overline{\mathcal{E}}_j(\theta) := E[|\Theta - \theta|^j]$ for shallow θ. If $\theta_1 < \theta \le \theta_0$, then by inspecting the graph on the left in Fig. 11 one obtains

$$|\Theta - \theta| \le \max\{\beta, \theta\} \le 3\beta/2 = 3K/2 + \mathcal{O}(K^3). \tag{5.6}$$

Therefore, $\overline{\mathcal{E}}_j(\theta) \le (3K/2)^j + \mathcal{O}(K^{j+2})$. If $\theta < \theta_1$, the estimate (4.11) gives

$$|\Theta - \theta| \le a(K)(8K\sin\theta)^{1/2}. \tag{5.7}$$

(Recall that $a(K)$ is very close to 1, as indicated above.) Therefore, $\overline{\mathcal{E}}_j(\theta) \le (8a(K)^2 K \sin\theta)^{j/2}$. For concreteness, assume that $K < 1$. Then, as indicated, $a(K) < 1.05$. If $\theta > \theta_0$, then $|\Theta - \theta| \le 2\beta$. Therefore,

$$\overline{\mathcal{E}}_j(\theta) \le \begin{cases} (2K)^j + \mathcal{O}(K^{j+2}) & \text{if } \theta_1 \le \theta \le \pi/2, \\ (9K\sin\theta)^{j/2} & \text{if } \theta < \theta_1, \end{cases} \tag{5.8}$$

which proves Theorem 2. (Theorem 1 also follows, as indicated in the introduction.)

For the sake of illustrating these estimates, we show the graphs of the first few moments for different values of K, obtained by numerical simulation of the billiard map and of P. See Figs. 6, 13, and 14. The graphs show $\mathcal{E}_j(\theta)/\gamma(K)$, where $\gamma(K)$ is the spectral gap of P, also obtained numerically. The relationship between the second moment and the spectral gap becomes particularly clear on the graphs. For $j = 1, 2, 3$ we consider curvature values $K = 2/3, 1/3, 1/6$. (The graph for $j = 2$ is shown in Fig. 6 at the beginning of the paper.) In order to minimize error at the end-angles 0 and π due to the $\cot\theta$ function, we have plotted the first moment times $\sin\theta$. The numerically obtained values for $\gamma(K)$ are $\gamma(2/3) = 0.1519$, $\gamma(1/3) = 0.0373$, $\gamma(1/6) = 0.0093$.

6 Conclusions

We prove that the classical scattering operator P associated to a class of random billiards with microstructure can be approximated by the standard Laplacian on the sphere S^2 when a curvature parameter of the microstructure is small. This suggests that the eigenfunctions and eigenvalues of P can be approximated by spherical harmonics and corresponding eigenvalues, and we provide numerical support for this.

Of special interest is the connection between the spectrum of P and scattering characteristics. We observe that the spectral gap of P is closely approximated by the second moment of scattering of P around the angle of incidence.

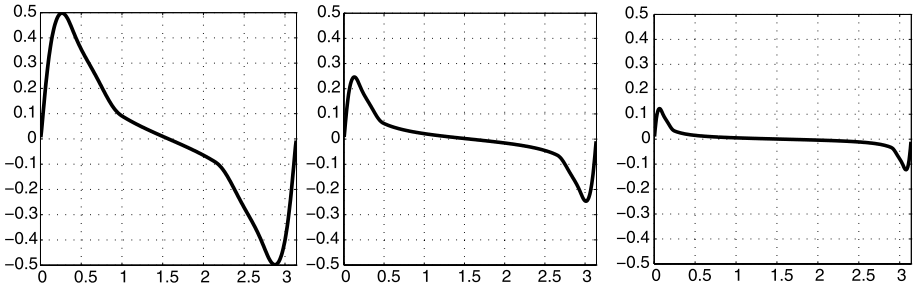

Fig. 14 The error term $\mathcal{E}_3(\theta)/\gamma(K)$ goes to zero as $K \to 0$. From left to right: $K = 2/3, 1/3, 1/6$

An elementary, but to the best of our knowledge new, observation suggesting that scattering processes of this kind in dimension 2 are connected to harmonic analysis on the 2-sphere is that the underlying deterministic billiard map T is naturally viewed as an area preserving map of S^2 for an arbitrary microstructure.

It is also interesting to interpret Theorem 1 from a stochastic differential equations viewpoint. The Markov chain on the interval $(0, \pi)$ defined by the Markov operator P jumps by small steps when K is small. In this case, it makes sense to approximate the discrete time process by a stochastic differential equation with infinitesimal generator $\mathcal{L} = \frac{1}{\sin\theta}\frac{d}{d\theta}(\sin\theta\frac{d\Phi}{d\theta})$:

$$P^{\lfloor t/\gamma(K)\rfloor} \approx e^{t\mathcal{L}}$$

and the limit process is governed by the stochastic differential equation

$$d\Theta_t = \frac{1}{2}\cot\Theta_t dt + dB_t,$$

where B_t is standard Wiener process. The cotangent function term provides a drift that goes to $+\infty$ as θ approaches 0, and to $-\infty$ as θ approaches π, so the process is bound to stay in $(0, \pi)$. As pointed out by the anonymous referee, this stochastic differential equation has the Knudsen cosine law as the (reversible) invariant probability distribution. We think that this continuous time process approximation, which is only indicated here without elaboration, merits further investigation.

Acknowledgements The second author is partially supported by an NSF grant. Most of this work was done during a visit by the first author to the University of Massachusetts, Amherst. He wishes to thank the department of mathematics for their warm hospitality.

References

1. Chernov, N., Markarian, R.: Chaotic Billiards. Mathematical Surveys and Monographs, vol. 127. AMS, Providence (2006)
2. Chernov, N., Dolgopyat, D.: Hyperbolic billiards and statistical physics. In: Proc. ICM, Madrid, Spain, vol. II, pp. 1679–1704. Eur. Math. Soc., Zurich (2006)
3. Comets, F., Popov, S., Schutz, G.M., Vachkovskaia, M.: Billiards in a general domain with random reflections. Arch. Ration. Mech. Anal. **191**, 497–537 (2009)
4. Feres, R.: Random walks derived from billiards. In: Hasselblatt, B. (ed.) Dynamics, Ergodic Theory, and Geometry. Mathematical Sciences Research Institute Publications, vol. 54, pp. 179–222 (2007)
5. Feres, R., Yablonsky, G.: Knudsen's cosine law and random billiards. Chem. Eng. Sci. **59**, 1541–1556 (2004)

6. Knudsen, M.: Kinetic Theory of Gases. Methuen's Monographs on Physical Subjects. London (1952)
7. Sinai, Ya.G.: Dynamical systems with elastic reflections. Ergodic properties of dispersing billiards. Russ. Math. Surv. **25**, 137–189 (1970)
8. Young, L.-S.: Statistical properties of systems with some hyperbolicity including certain billiards. Ann. Math. **147**, 585–650 (1998)